A New Concept for EEG/MEG Signal Analysis: Detection of Interacting Spatial Modes

Christian Uhl,* Frithjof Kruggel, Bertram Opitz, and D. Yves von Cramon

Max-Planck-Institute of Cognitive Neuroscience, D-04103 Leipzig, Germany

◆ ═══════════════════════════════════════ ◆

Abstract: We propose a new concept for analyzing EEG/MEG data. The concept is based on a projection of the spatiotemporal signal into the relevant phase space and the interpretation of the brain dynamics in terms of dynamical systems theory. The projection is obtained by a simultaneous determination of spatial modes and coefficients of differential equations. The resulting spatiotemporal model can be characterized by stationary points and corresponding potential field maps. Brain information processing can be interpreted by attraction and repulsion of spatial field distributions given by these stationary points. This allows an objective and quantitative characterization of the brain dynamics. We outline this concept and the underlying algorithm. Results of the application of this method to an event related potential (ERP) study of auditory memory processes are discussed. *Hum. Brain Mapping 6:137–149, 1998.*
© 1998 Wiley-Liss, Inc.

Key words: EEG/MEG; ERP/ERF components; spatial field distributions; dynamical systems; fixed points

◆ ═══════════════════════════════════════ ◆

INTRODUCTION

The analysis of electric and magnetic fields measured over the scalp surface is an important tool for gaining new insights into processes underlying phenomena such as cognitive processes, epileptic seizures, and sleep cycles. Basically, two complementary approaches are in use for investigating EEG/MEG data sets.

First, *spatial analyses* focus on the determination of characteristic spatial distributions and their interpretation in terms of different brain functions. Principal component analysis (PCA) [Donchin and Heffley, 1978] aims at representing the signal by spatial field distributions and corresponding amplitudes. The spatial microstate analysis [Lehmann, 1987] focuses on identifying quasistable field maps on the scalp surface and

their correspondence to brain information processing units. The extraction of cortical generators is the goal of source analysis. The underlying neuroelectromagnetic inverse problem possesses an infinite number of possible solutions, and therefore different approaches have been developed to narrow the solution space. A common approach to analyzing the neurophysiological signal is to model the source as current dipoles and to fit their placement, orientation, and strength to the data [Brenner et al., 1975; Scherg and von Cramon, 1986; Mosher et al., 1992]. More recent developments have focused on distributed solutions and the determination of current densities as generators of the measured signals [Hämäläinen and Ilmoniemi, 1984]. Other approaches suggest constraining the solution space by integrating spatial information from magnetic resonance imaging and positron emission tomography and extracting temporal information from EEG/MEG measurements [Dale and Sereno, 1993; Heinze et al., 1994; Fox and Woldorf, 1994; Belliveau et al., 1995].

Secondly, *temporal analyses* aim at identifying characteristic temporal sequences, with their interpretation again by means of different brain functions. This has led to characterizations in terms of ERP components as N100, P300, etc. More recent developments have aimed at characterizing time series by methods of dynamical systems theory, such as the evaluation of correlation dimensions and Lyapunov exponents [Babloyantz et al., 1985; Cerf et al., 1996] and coherences [Rappelsberger and Petsche, 1988; Schack and Krause, 1995].

These methods have been extensively used and revised and have revealed many interesting and important results.

However, there still remain uncertainties with these approaches, which are partly due to the separate (spatial *or* temporal) investigations neglecting the respective other component of the spatiotemporal signals. A particular problem in identifying ERP components and their corresponding dipole fits are due to the uncertainty of finding the correct time intervals describing different "brain states." PCA, which is usually performed on the entire data set, leads to orthogonal modes which are difficult to interpret if one considers more than one mode. However, PCA modes can be useful in getting an impression of the underlying dynamics and can be a good starting point for modeling EEG/MEG signals [Jirsa et al., 1994; Kelso and Fuchs, 1995], even if they are not necessarily the optimal choice for representing the dynamics of the signals.

The algorithm presented in Uhl et al. [1993, 1995] was a first attempt to fill the gap of separate spatial and temporal investigations by simultaneously fitting spatial distributions and coefficients describing the dynamics to given spatiotemporal signals. Our method was applied to EEG data sets of epileptic seizures [Friedrich and Uhl, 1996; Uhl and Friedrich, 1996] and MEG data of a motor-coordination task [Jirsa et al., 1995]. The mathematical and physical background of this approach is based on the theory of synergetics [Haken, 1983, 1987], a general concept describing complex self-organizing systems with emergent properties. The connection of this abstract theory to brain dynamics is reviewed elsewhere [Kelso, 1995; Nunez, 1995; Haken, 1996].

In this paper we outline the algorithm combining spatial and temporal approaches and present an interpretation of the obtained spatiotemporal model. This reveals unambiguous spatial modes (spatial field distributions) and corresponding time intervals describing brain dynamics, and therefore allows a more objective and quantitative interpretation of EEG/MEG data sets. In the next section, the link between complex dynamical systems and brain functioning is discussed. Our method for detecting spatial modes and their dynamics is presented thereafter (mathematical details are included in the appendices). In Example: Auditory ERP Study, our method will be applied to an example of an event-related potential (ERP) study with auditory stimuli, and the dynamics will be interpreted. Finally, we summarize the presented algorithm and the emerging impacts of such a concept.

COMPLEX DYNAMICAL SYSTEMS AND BRAIN FUNCTIONING

Synergetics

The theory of synergetics [Haken, 1983, 1987] provides a general concept describing complex self-organizing systems with emerging properties. The basis of this theory is a system consisting of a large number of nonlinearly interacting subsystems. Introducing a state vector Q with components Q_i describing the subsystem i, the evolution of the complex system can be described by a differential equation

$$\dot{Q}(t) = D[Q, c] + F(t) \qquad (1)$$

with a nonlinear vector function D, control parameters of the complex system c, and time-dependent fluctuating forces F(t). In the vicinity of critical values of the set of control parameters c, this high-dimensional complex system can be approximated by a low-dimensional set of order parameters, i.e., a low-dimensional superposition of state vectors V_i and time-dependent amplitudes $\xi_i(t)$:

$$Q \simeq \sum_i \xi_i(t)V_i \qquad (2)$$

The amplitudes $\xi_i(t)$ obey a set of differential equations, the so-called Langevin equations,

$$\dot{\xi}_i = d_i[[\xi_j]] + f_i(t) \qquad (3)$$

which can be derived analytically from the evolution equations (Eq. (1)).

For an elaborate presentation of this theory we refer the reader to Haken [1983, 1987].

Links of the theory of complex systems to brain dynamics and EEG/MEG signals

From a physical and neurophysiological point of view, the brain represents a very complex system

consisting of the order of 10^{11} interacting neurons. Therefore, concepts of the physical theory of complex dynamical systems have been applied to brain dynamics [Kelso, 1995; Nunez, 1995; Haken, 1996].

Since the evolution equations of the neurons and their interaction are not exactly known, EEG/MEG signals cannot rigorously be described by a bottom-up approach as sketched above. However, first attempts in this direction [Jirsa and Haken, 1996] have shown promising results.

In this paper we will present a top-down approach, i.e., an approach for obtaining from a measured EEG/MEG signal a decomposition into state vectors and time-dependent amplitudes and for obtaining the corresponding dynamics of the amplitudes. Our decomposition will be performed on the level of potentials/fields on the surface of the head: instead of conceiving of Eqs. (1–3) as equations of interacting neurons, one could transform these equations (if they were known) by Maxwell's theory of electromagnetism to equations describing dynamics of potentials/fields on the surface of the head.

Eq. (2) then reads

$$q(t) \simeq \sum_i x_i(t) v_i \qquad (4)$$

where q(t) represents the measured EEG/MEG signal: The vector components, $q_i(t)$, represent the time series of channel i of the EEG/MEG data set. The modes v_i represent spatial field distributions on the surface of the head. As an interaction of these modes we will assume the following type of differential equation:

$$\dot{x}_i = d_i[[x_j]] \qquad (5)$$

i.e., we neglect in this paper fluctuating forces, corresponding to the analysis of averaged EEG/MEG data sets, assuming that the fluctuating forces cancel out in the averaging process.

Below, we will present a method for obtaining the modes v_i and the vector function d_i, describing the dynamics of the amplitudes, and the first attempts to interpret these dynamics in terms of processing units in the brain.

Our approach to decomposing an EEG/MEG signal (Eq. (4)) and describing the dynamics (Eq. (5)) is closely related to answering the following questions concerning brain functioning:

1. Which regions in the brain do interact? This is answered on the level of field distributions on the surface of the head by the modes v_i or more precisely by certain linear combinations of them (so-called fixed points; see Interpretation of the Obtained Model, below).
2. How do these regions interact? The answer to this question is given by the dynamics (Eq. (5)) and an interpretation of the dynamics (see Interpretation of the Obtained Model, below).

The novelty of our approach is based on the following: we constrain our search for spatial field distributions by searching modes which interact in terms of differential equations. Thus, we take advantage of the high temporal resolution, which is one of the major advantages of EEG/MEG measurements, to draw conclusions from interacting spatial field distributions. So far, our method has only led to field distributions on the surface of the head. Further work should incorporate spatial dipole fits into this framework of constraining the associated dynamics to differential equations.

To avoid notional misunderstandings, we want to mention that *spatiotemporal* source localization techniques aim at solving the neuroelectromagnetic inverse problem by fitting spatial parameters to the data and describing the temporal evolution by amplitudes. Our spatiotemporal approach aims at fitting spatial and temporal parameters to the data set on the level of potential fields on the scalp surface, to find characteristics of underlying field distributions and their dynamics.

DETECTION OF INTERACTING SPATIAL MODES

Identification of spatial modes and their dynamics

Model of the dynamics

Close to instabilities, the function d_i, describing the interaction of the order parameters (Eq. (5)), can be expressed by low-dimensional polynomials, i.e.,

$$\dot{x}_i = d_i[[x_j]] = \sum_{j=1}^{N} a_{i,j}x_j + \sum_{j=1}^{N} \sum_{k=j}^{N} a_{i,jk}x_jx_k$$

$$+ \sum_{j=1}^{N} \sum_{k=j}^{N} \sum_{l=k}^{N} a_{i,jkl}x_jx_kx_l. \qquad (6)$$

The ansatz of a polynomial function is not stringent; under certain experimental conditions, other classes of functions can be considered, e.g., in the case of periodic observables within a trial [Haken et al., 1985], trigonometric basis functions can be considered.

To obtain the spatiotemporal model of the signal, i.e., the coefficients $a_{i,j}$, $a_{i,jk}$, and $a_{i,jkl}$ of Eq. (6) and the spatial distributions v_i of Eq. (4), we define a cost function, the global minimum of which represents the best choice of these parameters.

Cost function

The cost function C consists of a least square error function D of the dynamics given by Eq. (6) and a second term, $p \cdot V$, which is introduced to avoid ambiguities (see below):

$$C = D + p \cdot V \tag{7}$$

$$D = \sum_{i=1}^{N} \frac{\langle (\dot{x}_i - d_i[[x_j]])^2 \rangle}{\langle (\dot{x}_i)^2 \rangle}. \tag{8}$$

The appropriate number N of interacting spatial modes has to be guessed initially and confirmed or rejected by the obtained results (see Practical Strategy, below).

For $p = 0$ this cost function accords with the function presented in Uhl et al. [1995]. A similar cost function is used by Kwasniok [1996, 1997] to obtain a reduction of complex dynamical systems given by partial differential equations based on a methodology first pointed out by Hasselmann [1988].

The cost function aims at describing the dynamics in terms of differential equations. Since the cost function consists of a least-square-fit potential considering the time derivative, it is not optimally adapted to finding a differential equation which leads to the signal after numerical integration. Approaches aiming in this direction have to consider the right choice of initial conditions as well as coefficients describing the differential equations [Baake et al., 1992]. Since the data sets we are dealing with are averaged signals, but which still contain noise, it is not our goal to model the signal by numerical integration but to characterize the dynamics by approximated differential equations.

The cost function (7) has quite a large number of parameters to be fitted to the data sets:

$$D = D[x_i(t), a_{i,j}, a_{i,jk}, a_{i,jkl}]. \tag{9}$$

Next we will present how most of the parameters can be eliminated by analytic evaluation of partial variations.

Biorthogonal modes and the term V

To obtain the amplitudes $x_i(t)$ from the signal $q(t)$, a set of vectors u_i has to be introduced. A projection of the signal onto these vectors yields the amplitudes:

$$x_i(t) = u_i \cdot q(t). \tag{10}$$

Thus, the set of vectors u_i represents the set of the biorthogonal modes of v_i:

$$u_i \cdot v_j = \delta_{ij}. \tag{11}$$

By this projection procedure, temporal information of all channels is considered, which has been shown recently to quantify spatially extended dynamics more reliably than single-channel methods [Lachaux, 1997].

To avoid ambiguities, such as

$$x_i(t) \simeq x_j(t), \quad i \neq j,$$

the second term of the cost function, $p \cdot V$, consists of the absolute values of the scalar products:

$$V = \sum_{ij} |u_i \cdot u_j| \tag{12}$$

weighted by a scalar p.

The cost function now reads

$$C = C[u_i, a_{i,j}, a_{i,jk}, a_{i,jkl}]. \tag{13}$$

Elimination of parameters describing dynamics

Appendix A shows the variation of the cost function C with respect to $a_{i,j}$, $a_{i,jk}$, and $a_{i,jkl}$. As a result, these parameters can be written as a function of u_i:

$$a_{i,j}, a_{i,jk}, a_{i,jkl} = a_{i,j}, a_{i,jk}, a_{i,jkl}[u_i] \tag{14}$$

and therefore the cost function C depends on u_i only:

$$C = C[u_i]. \tag{15}$$

Normalization of modes and preprocessing of signal

For a further reduction of parameters, it is reasonable to project the signal $q(t)$ as a preprocessing step into a subspace, e.g., a subspace spanned by the principal component analysis (PCA) modes w_i of the averaged signals:

$$\tilde{q}(t) = \{\tilde{q}_i(t)\}_{i=1,\dots,s} \quad \text{with} \quad \tilde{q}_i = w_i \cdot q(t) \tag{16}$$

and search for modes $\tilde{u}_i$ in that subspace. The number s of vectors spanning the subspace should not be too small to show all relevant dynamics and components representing the signal.

The scaling of the vectors $\tilde{u}_i$ has to be fixed, which can be done by requiring

$$\langle x_i^2 \rangle = \langle (\tilde{q}\tilde{u}_i)^2 \rangle = c. \tag{17}$$

This is more reasonable than requiring $u_i^2 = c$, since our constraint (Eq. (17)) leads to cost functions dealing with comparable amplitudes and therefore comparable coefficients $a_{i,j}$, $a_{i,jk}$, and $a_{i,jkl}$. This can be solved by introducing generalized elliptic coordinates. The resulting nonlinear cost function C then depends on $\phi_i^{(j)}$ with $i = 1, \ldots, N$ representing the different spatial modes i, and $j = 1, \ldots, s - 1$ the different independent angles (see Appendix B).

The global minimum of this resulting cost function represents the best choice of spatial modes u_i and coefficients $a_{i,j}$, $a_{i,jk}$, and $a_{i,jkl}$ with respect to the least square fit defined by Eq. (7) describing the dynamics of the signal.

Minimization

Because of the nonlinear dependence of the resulting cost function on the angles $\phi_i^{(j)}$, numerical methods have to be considered for further calculation. The cost function depends on $N \cdot (s - 1)$ parameters, which is typical for low-dimensional signals ($N = 2 - 5$, $s = 5 - 10$) of the order 10–50. A great variety of algorithms for minimizing multidimensional cost functions exist, such as gradient-based algorithms, simulated annealing methods (e.g., Press et al. [1992]), and genetic algorithms [Holland, 1987]. For that order of dimensionality, genetic algorithms and simulated annealing techniques are more robust than gradient-based methods. We have found genetic algorithms in a number of optimization problems to give fast and reliable results [Kruggel and Lohmann, 1996]. However, any choice of optimization method is acceptable if it is able to deal with local minima in a 10–50 dimensional solution space.

Connection of spatial modes v_i with u_i

To obtain the spatial modes v_i from the biorthogonal modes u_i, Eq. (11) has to be inverted. However, the inverse is nonunique if the number N of modes u_i is smaller than the number s of PCA modes used for preprocessing. In Appendix C, a second cost function S is introduced to obtain a unique solution

$$v_i = v_i[u_j] \tag{18}$$

which is the best solution for representing the signal.

TABLE I. Strategy for finding right choice of number N of spatial modes spanning phase space and weight factor p of term p · V in cost function C
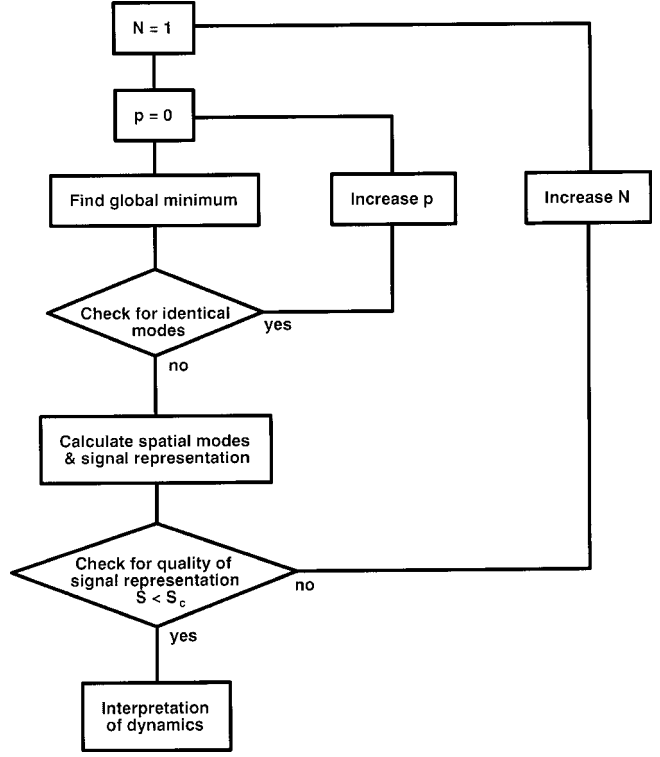
Practical strategy

We propose the strategy shown in Table I: a minimal number N of modes for representing the signal is guessed, and p is set to p = 0. The global minimum is calculated and the result is checked with respect to occurring identical biorthogonal modes u_i. In the case of occurrence, p is increased until the biorthogonal modes differ. Then the spatial modes v_i are calculated and the signal representation is checked by the cost function S (Appendix C). In the case of poor signal representation, the number of involved modes is increased until the representation is on an acceptable level.

The final step now consists of interpreting the obtained dynamics.

Interpretation of the obtained model

So far we have obtained a description of the signal in terms of a representation

$$q(t) = \sum_i x_i(t)v_i \tag{19}$$

and a model for the underlying dynamical system

$$\dot{x}_i = d_i[[x_j]]. \tag{20}$$

To gain more insight into the dynamics and to allow an interpretation by means of interaction of processing units, the dynamical system has to be analyzed.

Dynamical systems can be characterized by stationary points, so-called fixed points, which attract or repel trajectories in the space of the amplitudes, i.e., the phase space. The fixed points y_i are the points in phase space which do not evolve with time:

$$\dot{y}_i = 0. \tag{21}$$

Thus, they can be obtained by solving the nonlinear set of equations

$$d_i[[y_j]] = 0. \tag{22}$$

To obtain quantitative characteristics of these fixed points, the trajectory in the vicinity of these stationary points can be investigated by the so-called linear stability analysis (e.g., Haken [1983]). More sophisticated characteristics can be obtained by calculating not only time-invariant points but also time-invariant sets of points, such as limit cycles. These and more complicated aspects of dynamical systems theory are of course beyond the scope of this paper. We refer the interested reader to Guckenheimer and Holmes [1983].

However, we want to stress that already the characterization of the obtained dynamical system in terms of fixed points may be of great interest for an interpretation of the underlying processing. The spatial mode belonging to occurring attractive fixed points may be identified as a field representation on the scalp surface of processing units in the brain: a common definition of ERP/ERF components [Rösler, 1982] relies on positive or negative extrema of the time series:

$$q(t) = \text{extremal, i.e.,} \quad \frac{d}{dt}q(t) = 0 \tag{23}$$

due to extremal cortical activity represented by the component.

Our definition of processing units in terms of fixed points is similar. Considering the definition of fixed points (Eq. (21)) and the definition of the amplitudes (Eq. (10)), it is obvious that components correspond to

fixed points:

$$\left.\begin{array}{r} \dfrac{d}{dt}q(t) = 0 \\[2mm] y_i(t) = u_i \cdot q(t) \end{array}\right\} \Rightarrow \dfrac{d}{dt}y_i(t) = u_i \cdot \dfrac{d}{dt}q(t) = 0. \tag{24}$$

Fixed points are never reached by the trajectory, since the trajectory would stay there forever, but it is attracted and repelled by them. The discussion of fixed points, as shown, includes the discussion of components, but opens in addition a wide field of possible quantitative characterizations of the dynamics (representing the shape of the components, its strength of attraction and repulsion, etc.). This may also allow the detection of components in data sets (such as single-subject data) which are not detectable with the conventional approach, since additional irrelevant peaks uncorrelated with the processing of the experimental task may occur. Therefore, our method might lead to a more reliable definition of a component.

Identifying these fixed points and observing the trajectory in phase space being attracted in the course of time by different fixed points lead to a description of brain dynamics in terms of "successive" processing states. This can be conceived of as an analogy to spatial microstate analysis [Lehmann, 1987], but instead of stepping from one state into the next, our analysis leads to brain dynamics which are governed by changing attractions of different states.

This also leads to an impact on current dipole analyses, which face the problem of finding the right time interval of a commonly defined ERP/ERF component: either dipoles can be fitted directly to the stationary field which belongs to the fixed point representing a certain brain function, or else a time interval belonging to the influence of a fixed point can be obtained by studying the phase portrait, and the dipole fit can be applied to this defined time interval. The length of the time intervals belonging to the influence of the same fixed point for different stimuli is not necessarily of the same size and reflects different "durations" of the "same" brain function in different tasks.

For further discussions of the impact of this concept, refer to Conclusions, below.

EXAMPLE: AUDITORY ERP STUDY

Experiment

As an example for the application of our algorithm, we chose an auditory ERP study of Opitz and Mecklinger [1997]. That study was performed to examine

the neuronal and functional characteristics of processing deviancy and novelty in auditory stimuli. Three different stimuli were presented to 20 volunteers: standard (s), tone of 600 Hz; deviant (d), tone of 660 Hz; and novel (n), a novel sound selected from a class of unique sounds.

The deviant tones had to be counted (attend condition). During the experiment, 128-channel EEG recordings were carried out. The data sets were averaged for the different stimuli after artifact elimination, and bandpass (1–20 Hz) filtering. Figure 1 shows the time series (solid line) of electrode Fz for the three different conditions (the patterns in different time intervals will be discussed later). One observes a negative peak at 110 msec (the N100 component) in all three signals. Deviant and novel stimuli both show a strong positive peak between 250–400 msec (P300). Analysis of the signals should investigate the differences in processing deviant and novel stimuli in this time range. Below, we will discuss results of our proposed spatiotemporal analysis.

Spatiotemporal analysis

To allow a transparent comparison of the different cases, we fitted simultaneously the same biorthogonal modes u_i to the different datasets. Following the Practical Strategy (see above), we obtained $N = 2$ and $p = 0.1$ as a good choice (thereby, the optimization process needs less than 10 min computation time on a conventional workstation). Figure 2 shows the spatial modes v_1 and v_2 spanning the space of the relevant dynamics, and Table II shows the approximate values of the coefficients, describing the dynamics in terms of Equation (6). With these two modes, signal representation was achieved by 80–90% with respect to the $L_2 -$ norm. This representation is sufficient to leave the number of modes unchanged, given the fact that the resulting two-dimensional phase space allows a clear presentation of our concept, interpreting the dynamics.

Figure 3 shows graphic representations of the obtained dynamics (data sets of the standard condition, deviant condition, and novel condition). The axes represent the amplitudes of the corresponding spatial modes v_i (x_1-axis corresponds to v_1, x_2-axis to v_2). Each point in that space represents a different spatial field distribution: a linear combination of v_1 and v_2 weighted by the corresponding x_1 and x_2 values:
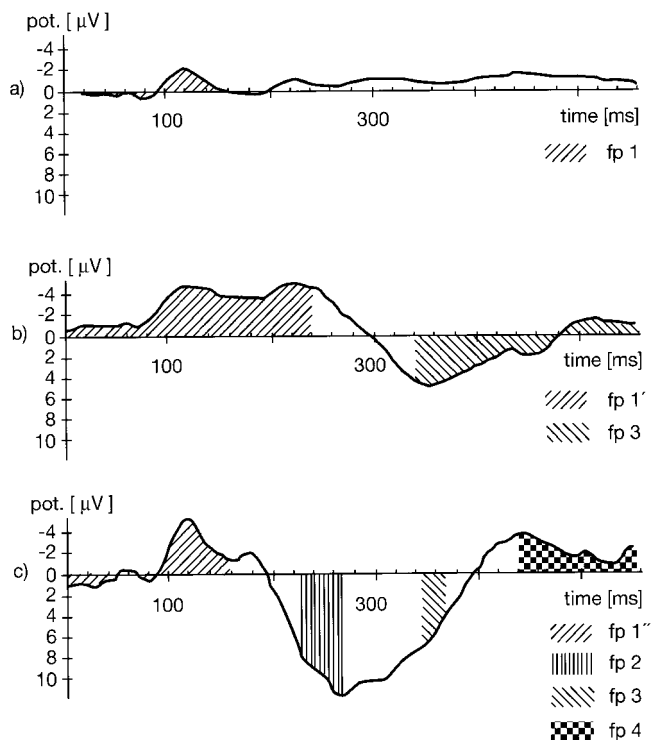
$$q = x_1 v_1 + x_2 v_2. \qquad (25)$$

Figure 1.
Time series of electrode Fz (reference: nose tip) for standard (**a**), deviant (**b**), and novel (**c**) conditions. The marked time intervals correspond to regions influenced by the fixed points (fp).

The scale of the axes is in principle arbitrary due to possible scaling of the modes:

$$q = (\alpha_1 x_1)(v_1/\alpha_1) + (\alpha_2 x_2)(v_2/\alpha_2).$$

The value of α has been fixed by the constraint

$$\langle x_1^2 \rangle = \langle x_2^2 \rangle = 10^{-4}$$

(see Normalization of Modes and Preprocessing of Signal, above). The solid thick line in Figure 3 represents the spatiotemporal signal in that space. (The observed trajectories cross each other. From a theoretical point of view this is incorrect, since there exists a unique solution for each initial condition of a dynamical system. The intersections are due to the projection into a two-dimensional subspace. A projection into a three-dimensional subspace leads to nonintersecting trajectories with a signal representation of 95–97%. However, for a more transparent presentation of our method, a two-dimensional projection was preferred, as these two-dimensional phase portraits represent approximations of the skeletons of the underlying dynamics.) We have marked the line every 40 msec to
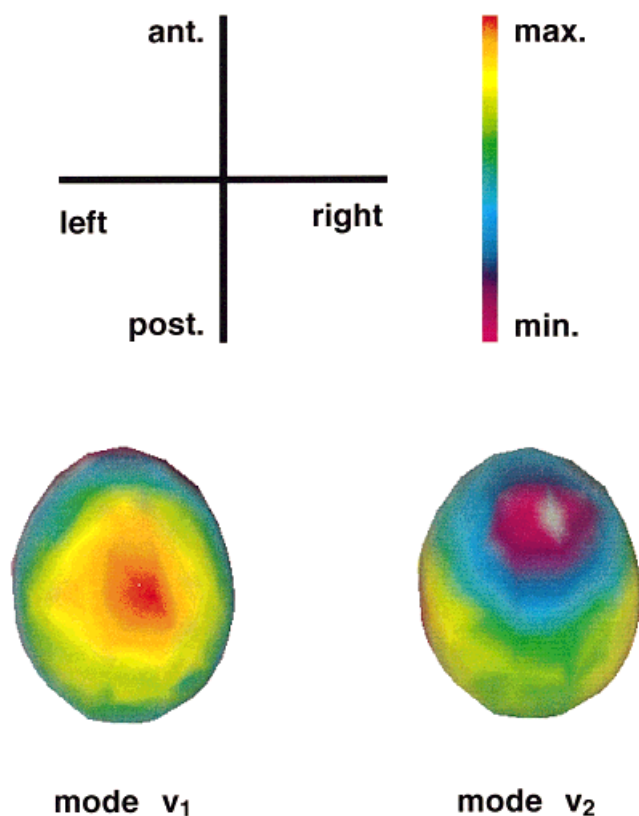
Figure 2.
Top row: Configuration of potential field maps and color coding. Bottom row: Spatial modes v_1 and v_2 spanning phase space, resulting from the minimization of the cost function of all three conditions. The modes represent spatial field distributions, configuration, and color coding as in the top row (v_1: minimum = 2.4 µV, maximum = 9.6 µV; v_2: minimum = −5.9 µV, maximum = 5.6 µV).

obtain a correspondence with the time series. The obtained set of differential equations predicts for each point in phase space the development of a trajectory in that point. The direction of the vector field is indicated by half-arrows in Figure 3, and the absolute value is indicated by color (red represents a small value: the trajectory remains longer in that region compared to the blue areas, i.e., large value). Finally, we plotted approximated fixed points (fp) calculated from the set of differential equations.

An interpretation of the observed spatiotemporal dynamics can be achieved from different perspectives.

Temporal interpretation

The following discussion of time intervals is also illustrated in Figure 1, where the time intervals have been included into the time series of the Fz-electrode.

In all three conditions (standard, deviant, and novel), the trajectory is first repelled by fixed point 0 (fp 0) and then influenced by fixed point 1 (fp 1, fp 1′, and fp 1″). The time range of the influence of fp 1 (fp 1′, fp 1″) varies from 0–160 msec (novel condition) up to 0–240 msec (deviant condition). The influence of fp 1 and the resulting trajectory is similar for all three conditions, and reveals the N100 component. After 200 msec for the standard condition, the trajectory is influenced by a number of additional fixed points. Most likely they correspond to artifacts and may be neglected, since the signal in that time domain does not represent significant changes.

In the cases of deviant and novel conditions, the trajectories behave differently: they both show a strong attraction by different fixed points, leading to P300 components. In the case of the deviant condition, the trajectory after 240 msec leaves the region of fp 1 and is strongly attracted by fp 3. This region is reached after 340 msec and the trajectory stays there up to 520 msec. The trajectory of the novel condition shows a different behavior: after 160 msec the trajectory is attracted by fp 2, reaches the region of that fixed point in the interval 230–270 msec, passes at 360 msec fp 3 of the deviant condition, and is finally attracted by fp 4 at 480–520 msec.

Spatial interpretation

Figure 4 presents the spatial field distributions corresponding to the occurring fixed points. The amplitude of these distributions is given by the distance of the fixed point to the origin. Therefore, the spatial information given by fp 0 can be neglected, and the amplitude is zero. Fp 1 and fp 1′ differ slightly but show similar field distributions, corresponding to the N100 field maps. Fp 1″ of the novel condition differs more, but taking the trajectory into account, one observes that fp 1′ of the deviant condition also seems to influence the novel case. Fp 2 and fp 3 differ clearly, indicating that different brain regions may be active. This confirms the findings of Opitz and Mecklinger [1997], where dipole analyses suggested different active cortical regions between 250–420 msec. The potential maps for this interval coincide with our findings of potential maps corresponding to fp 2 and fp 3. Fp 3 represents a fixed point of the deviant condition, but is also passed by the trajectory of the novel condition at the same time as in the deviant case. This suggests that in the novel condition as well, brain functions represented by fp 3 play a role in human brain information

TABLE II. Coefficients describing dynamics in terms of Eq. (6) obtained from the minimization of the cost function

Condition, mode i	Standard		Deviant		Novel	
	1	2	1	2	1	2
$a_{i,1}$	−32.3	36.2	2.00	−4.90	42.0	19.7
$a_{i,2}$	−32.3	−19.3	0.888	−2.22	−63.8	−29.0
$a_{i,11}$	−871.0	657.0	−9.31	28.4	−85.7	−19.7
$a_{i,12}$	−1,320.0	−107.0	25.1	−278.0	240.0	115.0
$a_{i,22}$	−194.0	275.0	−28.6	320.0	−278	−213.0
$a_{i,111}$	−3,010.0	2,310.0	90.0	18.3	41.0	9.65
$a_{i,112}$	−7,820.0	1,100.0	−424.0	261.0	−280.0	−96.2
$a_{i,122}$	−3,300.0	3,670.0	663.0	−756.0	−145.0	99.3
$a_{i,222}$	−856.0	291.0	−440.0	718.0	−512.0	−210.0

processing, but are less important than in the deviant case, an observation also noted by Mecklinger and Müller [1996]. The final ''processing unit'' of the novel case (fp 4) shows a distribution similar to that of fp 2. However, the strength is decreased.

Summarizing these findings, Figure 4 shows spatial field distributions ordered in the way of occurrence for the different stimuli. After the N100 component (fp 1), fp 3 in the deviant case becomes active; in the novel case, a processing unit represented by fp 2 is first activated before fp 3 and finally fp 4 are involved.

A final remark should be made about the presented analysis of the example. The two modes shown in Figure 2 span the subspace of the assumed relevant dynamics. Any linear combination of the two modes span the same space, i.e., an interpretation of the model should not be based on these modes, but on characteristics in that space, as we did by an interpretation of the dynamics in terms of fixed points: The spatial field distributions belonging to the fixed points are invariant under linear coordinate transformations in the subspace.

CONCLUSIONS

We have presented an algorithm which allows a projection of spatiotemporal EEG/MEG signals in a relevant subspace (relevant in terms of both dynamics and signal representation). The analysis of the dynamics in that subspace (the phase space) allows an objective and quantitative interpretation of the occurring phenomena in terms of attracting and repelling fixed points. This interaction of fixed points leads to an observation of potential field maps corresponding to different brain ''states,'' with changing influence on

information processing in the human brain. In contrast to spatial microstates [Lehmann, 1987], these ''states'' are not really occupied; rather, they are ''centers of attraction'' with changing influence on brain dynamics.

This new concept of the interpretation of EEG/MEG signals enables new quantitative approaches to obtaining a better understanding of information processing in the human brain:

Fitting dipoles to EEG/MEG signals does not rely on the choice of a time interval.
Interindividual differences can be investigated in terms of different values of attraction of fixed points.
Averaging trials may be improved by classifying individual trials into categories by their dynamics.

From our point of view, this leads to a new level of EEG/MEG analysis, since the basis of the interpretation of signals can be shifted from data-driven approaches (as in conventional analysis) to model-based approaches.

The presented method is limited to averaged signals, which show only small contributions in higher-frequency domains. This is due to limitations of calculating the time derivative of the signal and the neglect of fluctuating forces (compare Eq. (3) and Eq. (5)). The search for the global minimum of the nonlinear cost function is numerically more elaborate than calculating PCA modes by solving the linear eigenvalue problem of the correlation matrix. However, we gain a spatiotemporal model of the signal. Therefore, the main interpretation of the model is not to find differential equations which represent the signal after numerical integration, but to find a subspace which is dynamically relevant, to find invariants in that subspace as
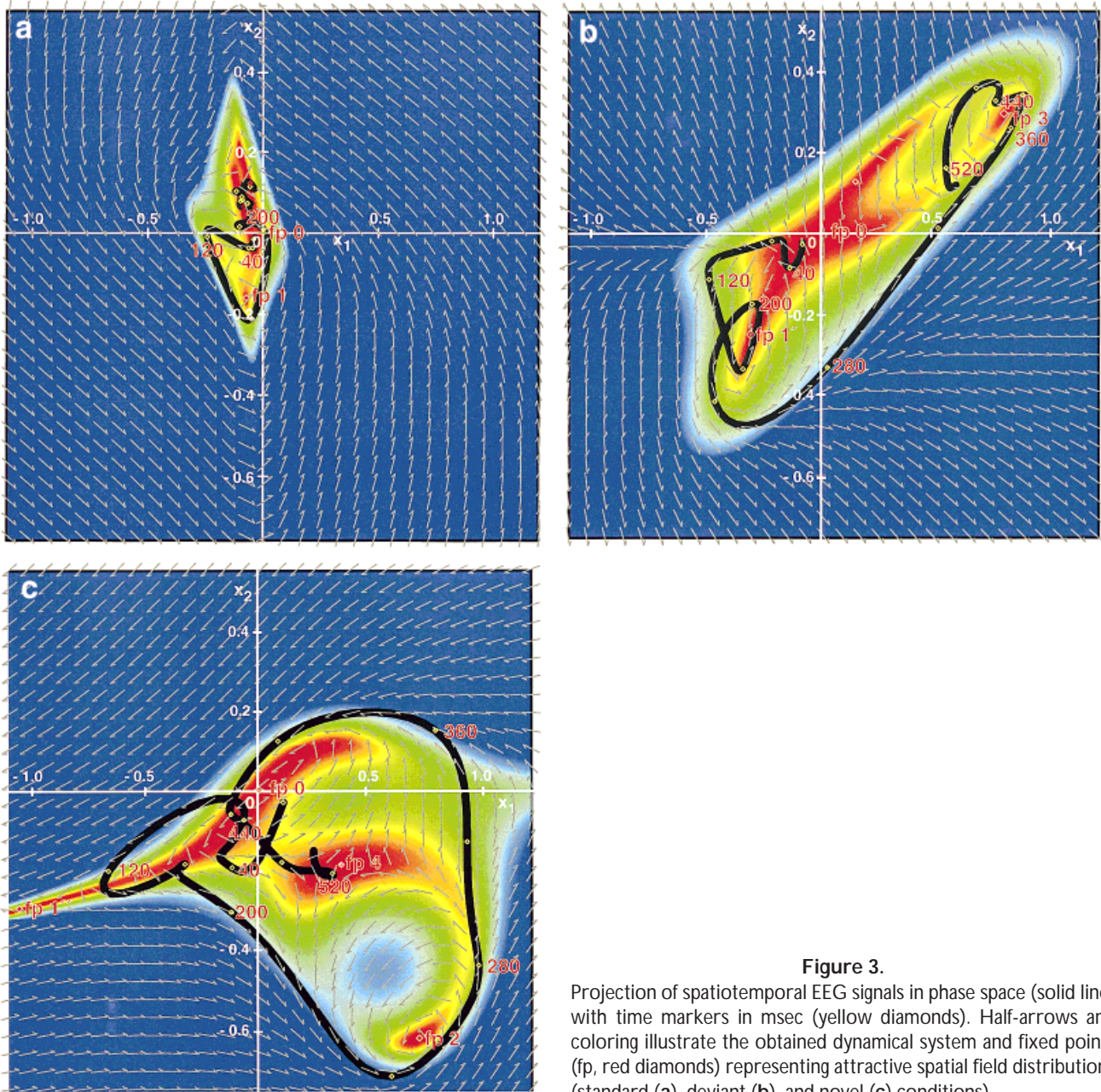
Figure 3.
Projection of spatiotemporal EEG signals in phase space (solid line) with time markers in msec (yellow diamonds). Half-arrows and coloring illustrate the obtained dynamical system and fixed points (fp, red diamonds) representing attractive spatial field distributions (standard (**a**), deviant (**b**), and novel (**c**) conditions).

given by the fixed points, and to find characteristics and interpretations of these invariants.

The justification of our approach is based on the theory of complex systems as described in Complex Dynamical Systems and Brain Functioning, above. Our first attempt at an interpretation of the dynamical systems in terms of fixed points showed links to the conventional identification of ERP/ERF components and to spatial microstate analysis, as discussed in Interpretation of the Obtained Model, above. Further investiga-

tions of ERP/ERF studies with the presented algorithm will lead to deeper insights into human brain information processing. In combination with more sophisticated methods of source localization, this will improve our knowledge of spatiotemporal brain dynamics.
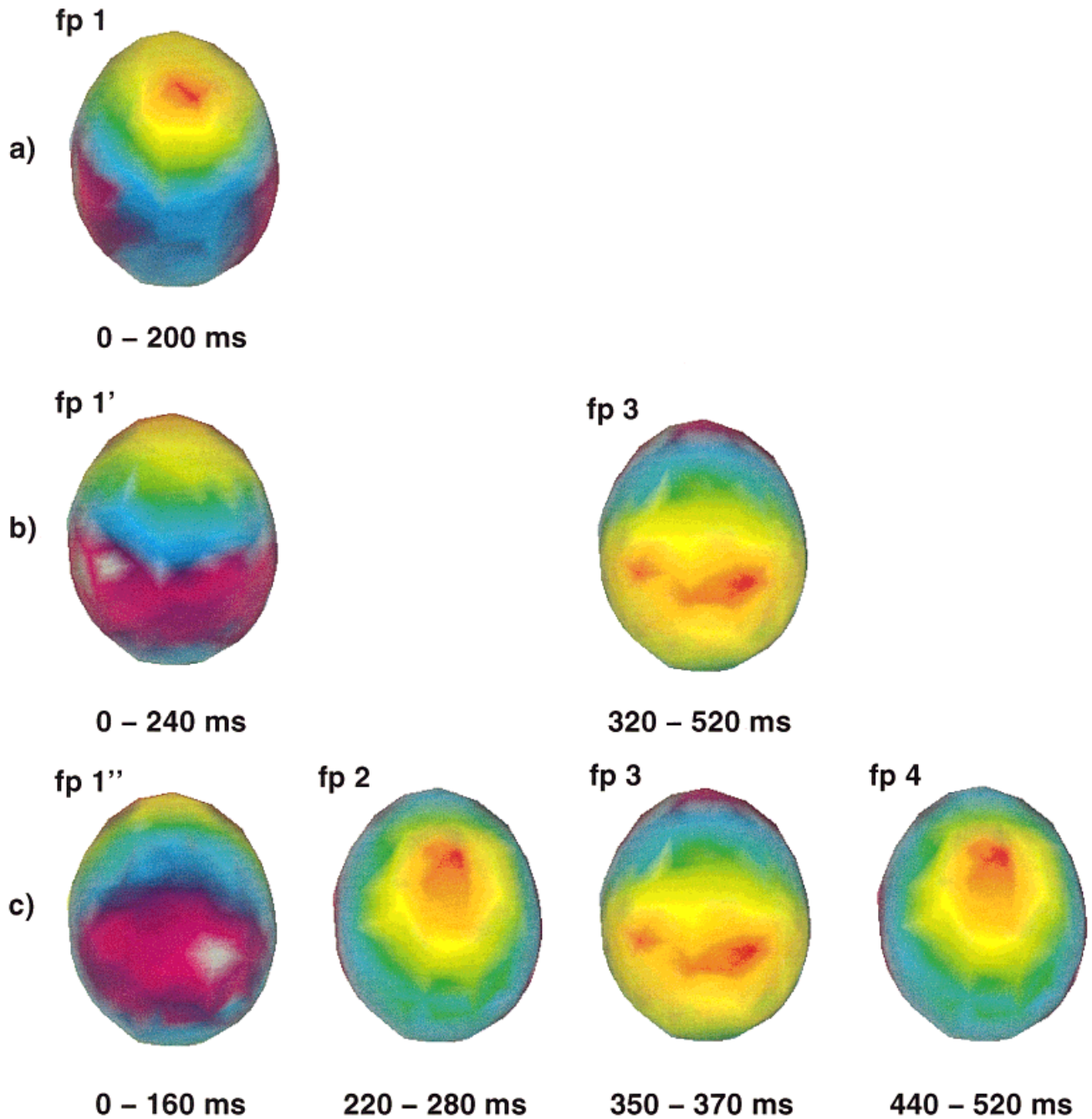
Figure 4.
Spatial field distributions corresponding to fixed points (fp) of phase portrait (standard (**a**), deviant (**b**), and novel (**c**) conditions). fp 1: minimum $= -1.23$ µV, maximum $= 0.32$ µV; fp 1': minimum $= -3.23$ µV, maximum $= -0.53$ µV; fp 1": minimum $= -9.94$ µV, maximum $= -2.66$ µV; fp 2: minimum $= 0.37$ µV, maximum $= 8.36$ µV; fp 3: minimum $= 1.89$ µV, maximum $= 7.54$ µV; fp 4: minimum $= 0.15$ µV, maximum $= 4.24$ µV (color coding and configuration as in top row of Fig. 2).

REFERENCES

Baake E, Baake M, Bock HG, Briggs KM (1992): Fitting ordinary differential equations to chaotic data. Phys Rev A 45:5524–5529.

Babloyantz A, Nicolis C, Salazar M (1985): Evidence of chaotic dynamics of brain activity during the sleep cycle. Phys Lett A 111:152–156.

Belliveau JW, Simpson GV, Baker JR, Huang-Hellinger FR, Wedeen VJ, George JS (1995): Dynamics of human brain mapping using simultaneous fMRI and EEG to model the electromagnetic forward problem. Hum Brain Mapping [Suppl] 3:88.

Brenner D, Williamson SJ, Kaufman L (1975): Visually evoked magnetic fields of the human brain. Science 190:480–482.

Cerf R, Sefrioui M, Toussaint M, Luthringer R, Macher JP (1996): Low-dimensional dynamic self-organization in δ-sleep: Effect of partial sleep deprivation. Biol Cybern 74:395–403.

Dale AM, Sereno MI (1993): Improved localization of cortical activity by combing EEG and MEG with MRI cortical surface reconstruction: A linear approach. J Cogn Neurosci 5:162–176.

Donchin E, Heffley E (1978): Multivariate analysis of event-related potential data: A tutorial review. In: Otto D (ed): Multidisciplinary Perspectives in Event-Related Potential Research (EPA-600/9-77-043). Washington, DC: U.S. Government Printing Office.

Fox PT, Woldorff MG (1994): Integrating human brain maps. Curr Opin Neurobiol 4:151–156.

Friedrich R, Uhl C (1996): Spatio-temporal analysis of human electroencephalograms: Petit-mal epilepsy. Physica D 98:171–182.

Guckenheimer J, Holmes PJ (1983): Nonlinear Oscillations, Dynamical Systems, and Bifurcations of Vector Fields. Berlin: Springer-Verlag.

Haken H (1983): Synergetics. An Introduction, 3rd ed. Berlin: Springer-Verlag.

Haken H (1987): Advanced Synergetics, 2nd ed. Berlin: Springer-Verlag.

Haken H (1996): Principles of Brain Functioning, Berlin: Springer-Verlag.

Haken H, Kelso JAS, Bunz H (1985): A theoretical model of phase transitions in human hand movements. Biol Cybern 51:347–356.

Hämäläinen MS, Ilmoniemi RJ (1984): Interpreting Measured Magnetic Fields of the Brain: Estimates of Current Distributions. Technical Report TKK-F-A559, Helsinki University of Technology.

Hasselmann K (1988): PIPs and POPs: The reduction of complex dynamical systems using principal interaction and oscillation patterns. J Geophys Res 93:11015–11021.

Heinze HJ, Mangun GR, Burchert W, Hinrichs H, Scholz M, Münte TF, Gös A, Scherg M, Johannes S, Hundeshagen H, Gazzangia MS, Hillyard SA (1994): Combined spatial and temporal imaging of brain activity during visual selective attention in humans. Nature 372:543–546.

Holland JH (1975): Adaption in Natural and Artificial Systems, Ann Arbor: Michigan University Press.

Jirsa VK, Haken H (1996): Field theory of electromagnetic brain activity. Phys Rev Lett 77:960–963.

Jirsa VK, Friedrich R, Haken H, Kelso JAS (1994): A theoretical model of phase transitions in the human brain. Biol Cybern 71:27–35.

Jirsa VK, Friedrich R, Haken H (1995): Reconstruction of the spatio-temporal dynamics of a human magnetoencephalogram. Physica D 89:100–122.

Kelso JAS (1995): Dynamic Patterns. The Self-Organization of Brain and Behavior, Cambridge: MIT Press.

Kelso JAS, Fuchs A (1995): Self-organizing dynamics of the human brain: Critical instability and Shilnikov chaos. Chaos 5:64–69.

Kruggel F, Lohmann G (1996): A toolkit for the analysis of multimodal brain data sets. In: Lembke HV, Inamura K, Jaffe CC, Vannier MW (eds): Computer Assisted Radiology (CAR 96). Berlin: Springer Verlag, pp 323–328.

Kwasniok F (1996): The reduction of complex dynamical systems using principal interaction patterns. Physica D 92:28–60.

Kwasniok F (1997): Optimal Galerkin approximations of partial differential equations using principal interaction patterns. Phys Rev E 55:5365–5375.

Lachaux J-P, Pezard L, Garnero L, Pelte C, Renault B, Varela FV, Martinerie J (1997): Spatial extension of brain activity fools the single-channel reconstruction of EEG dynamics. Hum Brain Mapping 5:26–47.

Lehmann D (1987): Principles of spatial analysis. In: Gevins AS, Remond A (eds): Methods of Brain Electrical and Magnetic Signals. Handbook of Electroencephalography and Clinical Neurophysiology, Revised Series, Volume 1. Amsterdam: Elsevier pp 309–354

Mecklinger A, Müller N (1996): Dissociations in the processing of ''what'' and ''where'' information in working memory: An event-related potential analysis. J Cogn Neurosci 8:453–473.

Mosher JC, Lewis PS, Leahy RM (1992): Multiple dipole modeling and localization from spatio-temporal MEG data. IEEE Trans Biomed Eng 39:541–557.

Nunez PL (1995): Experimental connections between EEG data and the global wave theory. In: Nunez PL (ed): Neocortical Dynamics and Human EEG Rhythms. Oxford: Oxford University Press pp 534–590.

Opitz B, Mecklinger A (1997): What are the similarities in hearing cars and tones? Fourth Annual Meeting of the Cognitive Neuroscience Society, March 23–25, Boston, Massachusetts.

Press WH, Teukolsky SA, Vetterling WT, Flannery BP: Numerical Recipes in C, 2nd ed. Cambridge, UK: Cambridge University Press.

Rappelsberger P, Petsche H (1988): Probability mapping: Power and coherence analyses of cognitive processes. Brain Topogr 1:46–54.

Rösler F (1982): Hirnelektrische Korrelate Kognitiver Prozesse, Berlin: Springer-Verlag.

Schack B, Krause W (1995): Dynamic power and coherence analysis of ultra short-term cognitive processes—A methodical study. Brain Topogr 8:127–136.

Scherg M, von Cramon DY (1986): Evoked dipole source potentials of the human auditory cortex. Electroencephalogr Clin Neurophysiol 65:344–360.

Uhl C, Friedrich R (1996): Spatio-temporal signal analysis with applications to EEG-analysis. Neuroimage [Suppl] 3:260.

Uhl C, Friedrich R, Haken H (1993): Reconstruction of spatio-temporal signals of complex systems. Z Phys B 92:211–219.

Uhl C, Friedrich R, Haken H (1995): Analysis of spatio-temporal signals of complex systems. Phys Rev E 51:3890–3900.

APPENDIX A

Eq. (6) can be rewritten as

$$\dot{x}_i = \sum_{\alpha=1}^{M} a_{i,\alpha} \xi_{i,\alpha} \tag{26}$$

after introduction of abbreviations

$$\left\{a_{i,\alpha}\right\}_{\alpha=1,...,M} = \left\{\left\{a_{i,j}\right\}_{j=1,...,N}, \quad \left\{a_{i,jk}\right\}_{j=1,...,N;k=j,...,N},\right.$$
$$\left.\cdot \left\{a_{i,jkl}\right\}_{j=1,...,N;k=j,...,N;l=k,...,N}\right\}$$

$$\left\{\xi_{i,\alpha}\right\}_{\alpha=1,...,M} = \left\{\left\{x_j\right\}_{j=1,...,N}, \quad \left\{x_j x_k\right\}_{j=1,...,N;k=j,...,N},\right.$$
$$\left.\cdot \left\{x_j x_k x_l\right\}_{j=1,...,N;k=j,...,N;l=k,...,N}\right\}. \tag{27}$$

The cost function D then reads

$$D = \sum_{i=1}^{N} \frac{\left\langle \left(\dot{x}_i - \sum_{\alpha=1}^{M} a_{i,\alpha}\xi_{i,\alpha}\right)^2 \right\rangle}{\left\langle \dot{x}_i^2 \right\rangle}. \tag{28}$$

Variation with respect to $a_{j,\beta}$ yields

$$\frac{\partial C}{\partial a_{j,\beta}} = \frac{\partial D}{\partial a_{j,\beta}} = 0 \Rightarrow \sum_{\alpha=1}^{M} \left\langle \xi_{j,\alpha}\xi_{j,\beta}\right\rangle a_{j,\alpha} = \left\langle \dot{x}_j\xi_\beta\right\rangle \tag{29}$$

which can be solved by

$$a_i = Q_i^{-1} b_i \tag{30}$$

with $(a_i)_\alpha = a_{i,\alpha}, (Q_i)_{\alpha\beta} = \left\langle \xi_{i,\alpha}\xi_{i,\beta}\right\rangle, (b_i)_\beta = \left\langle \dot{x}_i\xi_{i,\beta}\right\rangle. \tag{31}$

Inserting this expression back into D leads to

$$D = N - \sum_{i=1}^{N} \frac{b_i Q_i^{-1} b_i}{\left\langle \dot{x}_i^2 \right\rangle}. \tag{32}$$

Because of Eq. (27) and (10), this depends on the biorthogonal modes u_i only.

APPENDIX B

We utilize the constraint of a fixed contribution of a mode to the signal

$$\left\langle x_i^2 \right\rangle = \left\langle (\tilde{q}\tilde{u}_i)^2 \right\rangle = c \tag{33}$$

with the signal $\tilde{q}(t)$ in PCA projection:

$$q(t) = \sum_{j=1}^{s} \eta_j w_j \Rightarrow \tilde{q}(t) = \left\{\eta_j\right\}_{j=1,...,s}. \tag{34}$$

Because of $\left\langle \eta_i\eta_j\right\rangle = \delta_{ij}$ the constraint then reads:

$$\left\langle (\tilde{q}\tilde{u}_i)^2 \right\rangle = \sum_{j=0}^{s} \left\langle \xi_j^2 \right\rangle (\tilde{u}_i^{(j)})^2 = c \tag{35}$$

which represents an s-dimensional ellipsoid. This can be solved by generalized elliptic coordinates:

$$u_i^{(1)} = r^{(1)} \cos \phi_i^{(1)} \tag{36}$$

$$u_i^{(j)} = r^{(j)} \cos \phi_i^{(j)} \prod_{k=1}^{j-1} \sin \phi_i^{(k)} \quad \text{if} \quad j \neq 1, s \tag{37}$$

$$u_i^{(s)} = r^{(s)} \prod_{k=1}^{s-1} \sin \phi_i^{(k)} \tag{38}$$

with

$$r^{(j)} = \sqrt{c/\left\langle \eta_j^2 \right\rangle}. \tag{39}$$

APPENDIX C

The cost function S to obtain the modes v_i from u_i is defined by the function:

$$S = \frac{\left\langle \left(q(t) - \sum_i x_i(t)v_i\right)^2 \right\rangle}{\left\langle (q(t))^2 \right\rangle}$$

$$= \frac{\left\langle \left(q(t) - \sum_i (u_i \cdot q(t))v_i\right)^2 \right\rangle}{\left\langle (q(t))^2 \right\rangle} \tag{40}$$

which is the natural cost function concerning an optimal signal representation with respect to the least-variance norm.

Variation of S with respect to v_j yields

$$\frac{\partial S}{\partial v_j} = 0 \Rightarrow \sum_{i=1}^{N} \left\langle x_i x_j\right\rangle v_j = \left\langle q x_j\right\rangle \tag{41}$$

which can be inverted to

$$v_j[u_i] = \sum_{i=1}^{N} M_{ij}^{-1}\left\langle q x_i\right\rangle = \sum_{i=1}^{N} M_{ij}^{-1}(\left\langle q \otimes q\right\rangle u_i) \tag{42}$$

with $M_{ij} = \left\langle x_i x_j\right\rangle = u_i\left\langle q \otimes q\right\rangle u_j$, and $\otimes$ representing a dyadic product.

To proof Eq. (11), $v_j \cdot u_k$ is calculated:

$$v_j \cdot u_k = \sum_{i=1}^{N} M_{ij}^{-1} u_k \left\langle q \otimes q\right\rangle u_i \tag{43}$$

$$= \sum_{i=1}^{N} M_{ij}^{-1} M_{ki} = \delta_{jk}. \tag{44}$$